Supplement of Clim. Past, 20, 313–333, 2024
https://doi.org/10.5194/cp-20-313-2024-supplement

Climate of the Past
Open Access
EGU

Supplement of

State-dependent impact of major volcanic eruptions observed in ice-core records of the last glacial period

Johannes Lohmann et al.

Correspondence to: Johannes Lohmann (johannes.lohmann@nbi.ku.dk)

S1. ADJUSTMENT OF ERUPTION TIMES FROM STACKED SULFATE PEAKS

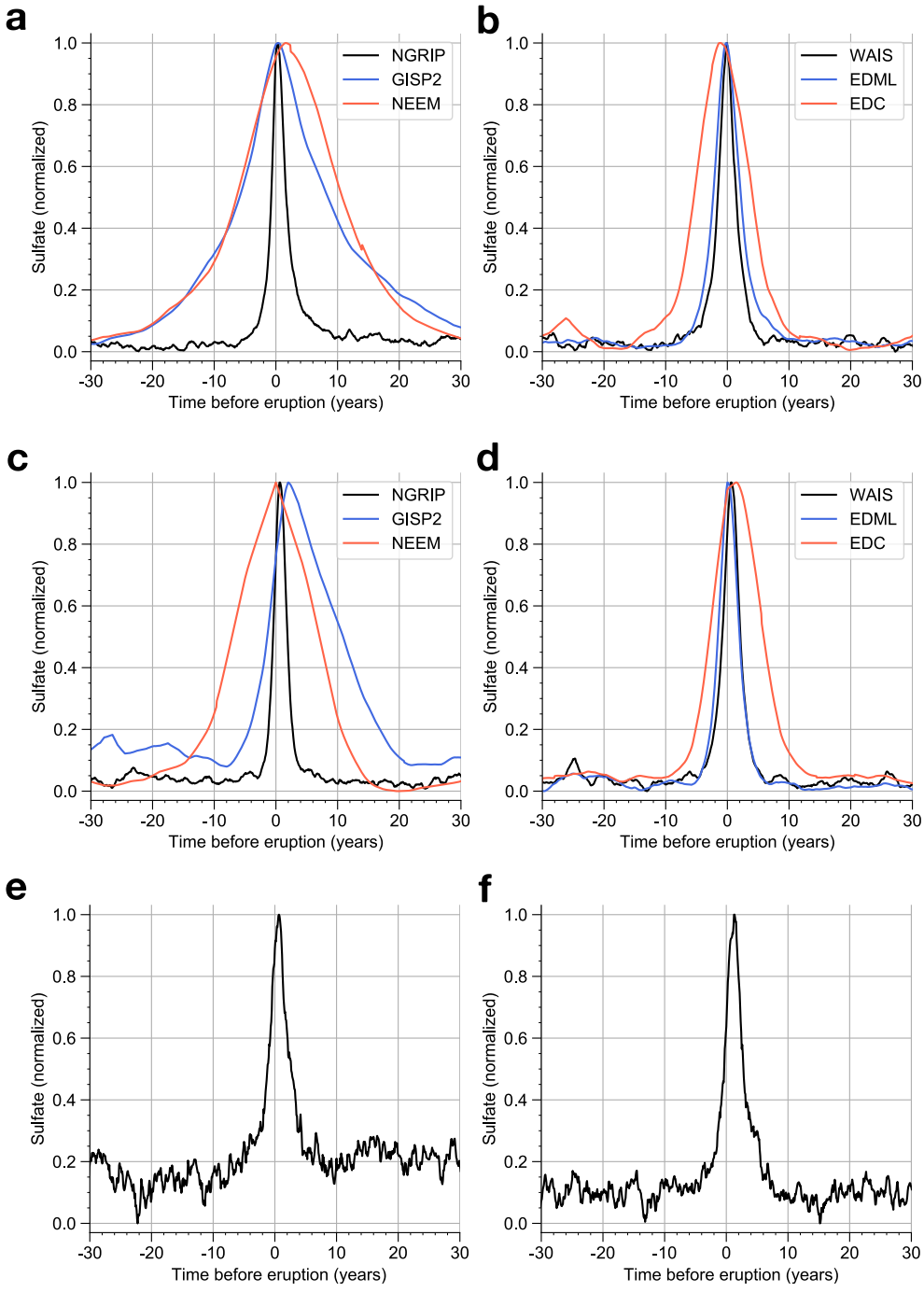

FIG. S1. **a-b** Average sulfate signal in the NGRIP[1], GISP2[2], NEEM[3], WAIS[4], EDML[5] and EDC[5] cores aligned to the nominal ages of the unipolar eruptions as derived from the depths given in Lin et al. (2022)[1]. **c-d** Same, but for the bipolar eruptions aligned to the ages derived from the depths in Svensson et al. 2020. **e-f** ECM signal in the WAIS core[6], aligned at the bipolar (**e**) and unipolar (**f**) eruptions.

As explained in the main text, we adjust the timings of the eruptions derived from the nominal depths of Svensson et al. (2020)[7] and Lin et al. (2022)[1] such that the average sulfate peaks of the eruptions in all cores are aligned. This is done because when using the ages derived from the nominal depths and plotting the average sulfate signals centered around all eruptions in each core, one can see small but significant systematic offsets in many of the cores, as shown in Fig. S1. For the WAIS ice core, we furthermore use the electrical conductivity measurements (ECM) shown in Fig. S1e-f, which also record the volcanic eruptions and reveal a more significant systematic offset. Based on these offsets, we shift all bipolar eruption ages back in time by 0.5 years in NGRIP and GISP2, by 2 years in NEEM, and by 0.7 years in WAIS. For EDC the bipolar eruption ages are shifted forward in time by 1 year. For the unipolar eruptions, we shift the ages back in time by 2 years in GISP2, 1 year in NGRIP, 1.5 years in EDC and 2.2 years in WAIS. No shift is applied to GRIP, since no data of sufficient quality is available.

One can further see that some records have very wide average peaks. These are the cores where the sulfur records have a relatively low measurement resolution, as listed in Tab. S1. As a result, instead of trying to estimate the start of the eruption from the start of the sulfate peaks, we add a constant offset as an estimate for the time delay from the true start of the eruption to maximum sulfur deposition in the ice core (see main text). Since these two steps led to a shaper and more well-aligned isotopic response, they seem justified even though they cannot fully achieve a perfect alignment of the eruptions along their true starting age.

TABLE S1. Median time resolution of sulfate records (in years)

Ice core	**9-11.7 ka**	**11.7-20 ka**	**20-30 ka**	**30-40 ka**	**40-50 ka**	**50-60 ka**
NGRIP	0.016	0.038	0.056	0.056	0.057	0.059
NEEM	9.9	9.9	10.1	10.0	10.0	10.0
GISP2	2.1	4.7	11.5	10.1	13.8	15.5
WAIS	0.10	0.13	0.31	0.41	0.53	0.71
EDC	1.2	1.9	3.2	3.7	1.9	1.6
EDML	1.2	0.5	0.8	0.9	1.0	1.1

Due to the variation of the annual layer thickness in the ice core, the widths of the sulfate peaks, and thus the precision of the eruption age estimates can depend strongly on the age of the eruption (as a result of layer thinning with depth) and the climate state (as a result of changes in accumulation rate). In Fig. S2a,b this is demonstrated for the GISP2 core. The decreasing layer thickness with age leads to a wider average sulfate peak for older eruptions (panel a). The lower accumulation rate

during stadial periods leads also to a wider sulfate peak compared to the interstadial periods (panel b).

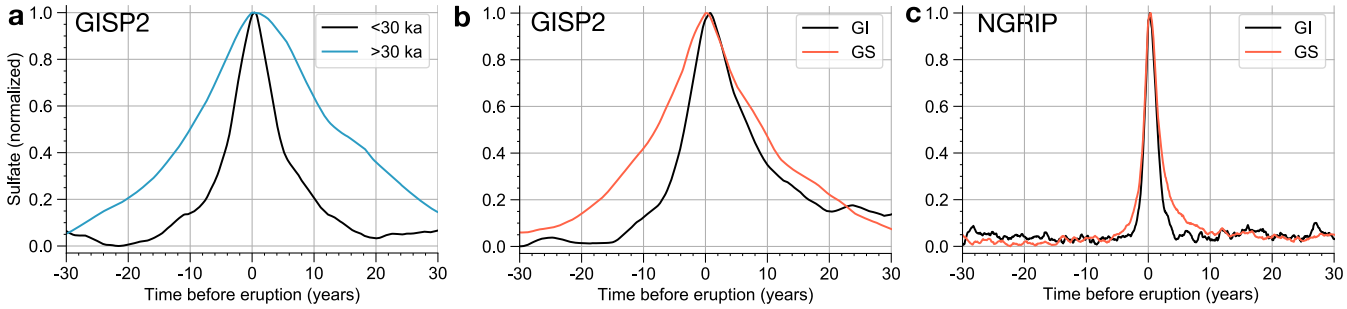

FIG. S2. **a,b** Average sulfate signal in the GISP2 ice cores aligned to the nominal ages of the bipolar eruptions as derived from the depths given in Svensson et al (2020). In panel **a** the data set is split up into eruptions occurring before and after 30 ka. Panel **b** shows the average sulfate signal for bipolar eruptions occurring during Greenland interstadials (GI) and Greenland stadials (GS). **c** Same as **b**, but for NGRIP.

S2. FURTHER SUPPLEMENTAL FIGURES

[1] J. Lin, A. Svensson, C. S. Hvidberg, J. Lohmann, S. Kristiansen, D. Dahl-Jensen, J. P. Steffensen, S. O. Rasmussen, E. Cook, H. A. Kjær, B. M. Vinther, H. Fischer, T. Stocker, M. Sigl, M. Bigler, M. Severi, R. Traversi, and R. Mulvaney, Clim. Past. **18**, 485 (2022).

[2] P. A. Mayewski, L. D. Meeker, M. S. Twickler, S. Whitlow, Q. Yang, W. B. Lyons, and M. Prentice, J. Geoph. Research **102**, 26345 (1997).

[3] S. Schüpbach *et al.*, Nature Comm. **9**, 1476 (2018).

[4] M. Sigl *et al.*, Clim. Past **12**, 769 (2016).

[5] M. Severi *et al.*, Clim. Past **3**, 367 (2007).

[6] T. J. Fudge, B. R. Markle, K. M. Cuffey, C. Buizert, K. C. Taylor, E. J. Steig, E. D. Waddington, H. Conway, and M. Koutnik, Geophys. Res. Lett. **43**, 3795 (2016).

[7] A. Svensson *et al.*, Clim. Past **16**, 1565 (2020).

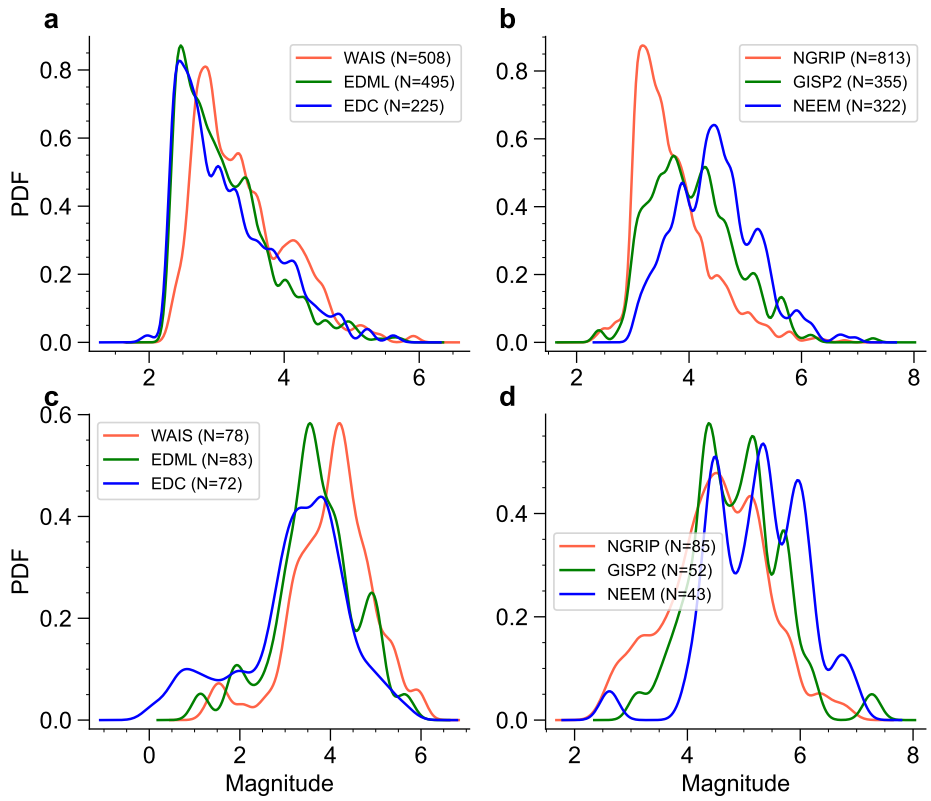

FIG. S3. Distributions of the sulfate deposition magnitude in the individial ice cores for the unipolar (**a, b**) and bipolar (**c, d**) data sets. The magnitude is defined as the logarithm of the sulfate deposition (in kg/km^2) in the individual cores, estimated by Lin et al. (2022).

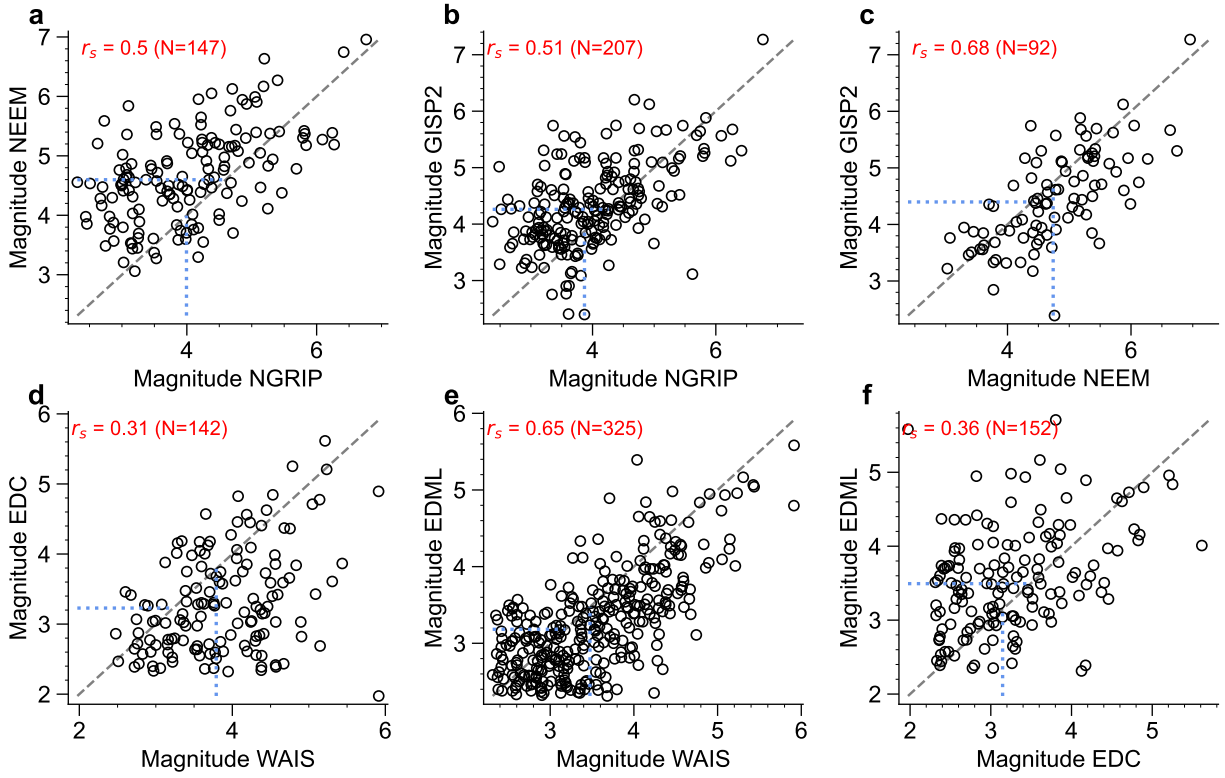

FIG. S4. Correlation of the sulfate deposition magnitude in pairs of cores for the subset of eruptions of the unipolar data set, which have been identified in both cores. In red we give the Spearman correlation. The gray dashed line is the identity line, and the mean values are given by the dotted blue lines. From the Greenland data (**a-c**) it is seen that NEEM and GISP2 show clearly higher average deposition values compared to NGRIP. The NEEM deposition values are slightly higher than those in GISP2. The Antarctic data (**a-c**) shows that WAIS has the highest average deposition values. The deposition in EDML is slightly larger compared to EDC.

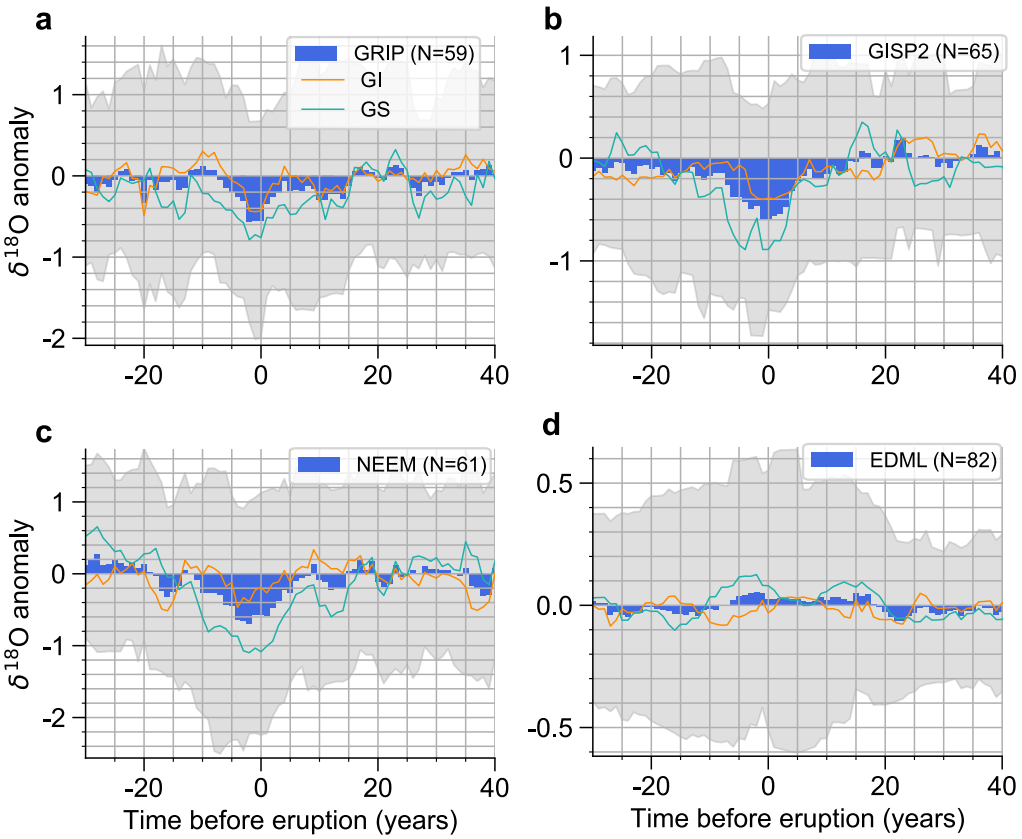

FIG. S5. Average δ^{18}O anomaly (permil) in 4 ice cores centered at the bipolar eruptions, defined with respect to the mean of the period 10-50 years prior. The average signal is shown in blue, and the gray bands are the 16- to 84-percentiles of detrended time slices covering individual eruptions. In orange (green) we show the mean signal of eruptions during GI (GS). Not all 82 bipolar eruptions were detected in the volcanic records of all cores by Svensson et al. (2020). Here we only consider eruptions in each core where a specific depth is given in Svensson et al. (2020), and the number of eruptions where this is the case is given in the captions of the panels.

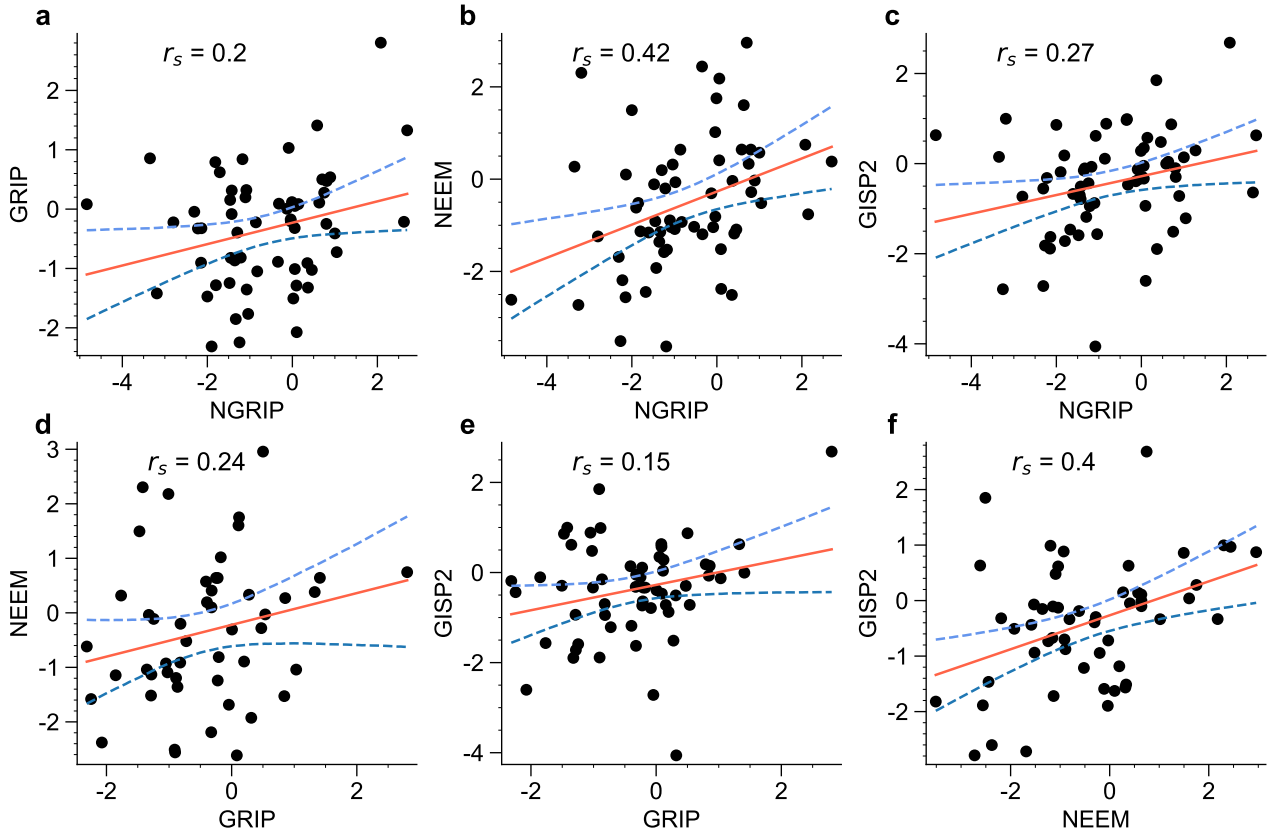

FIG. S6. Pairwise correlation of the 6-year average δ^{18}O anomalies (permil) in individual Greenland cores. The 6-year period consists of the year of the eruption as well as the following five years. Shown is the data (black) along with a linear regression (red) and an associated 95% confidence band (blue). Furthermore, the Spearman correlation coefficient is given.

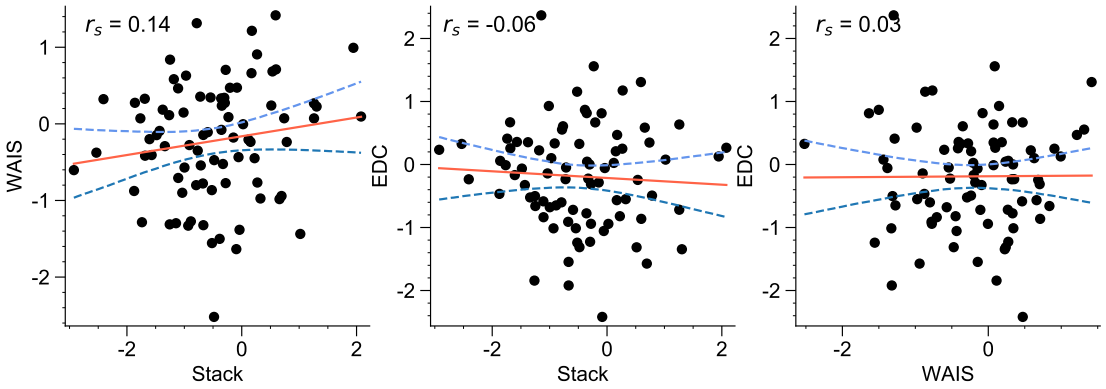

FIG. S7. Pairwise correlation of the average δ^{18}O anomalies (permil) in the Greenland stack (6-year average) and the Antarctic WAIS and EDC cores cores. For WAIS and EDC the period to define the average anomaly is 4 and 14 years, respectively, as explained in the main text. Shown is the data (black) along with a linear regression (red) and an associated 95% confidence band (blue). Furthermore, the Spearman correlation coefficient is given.

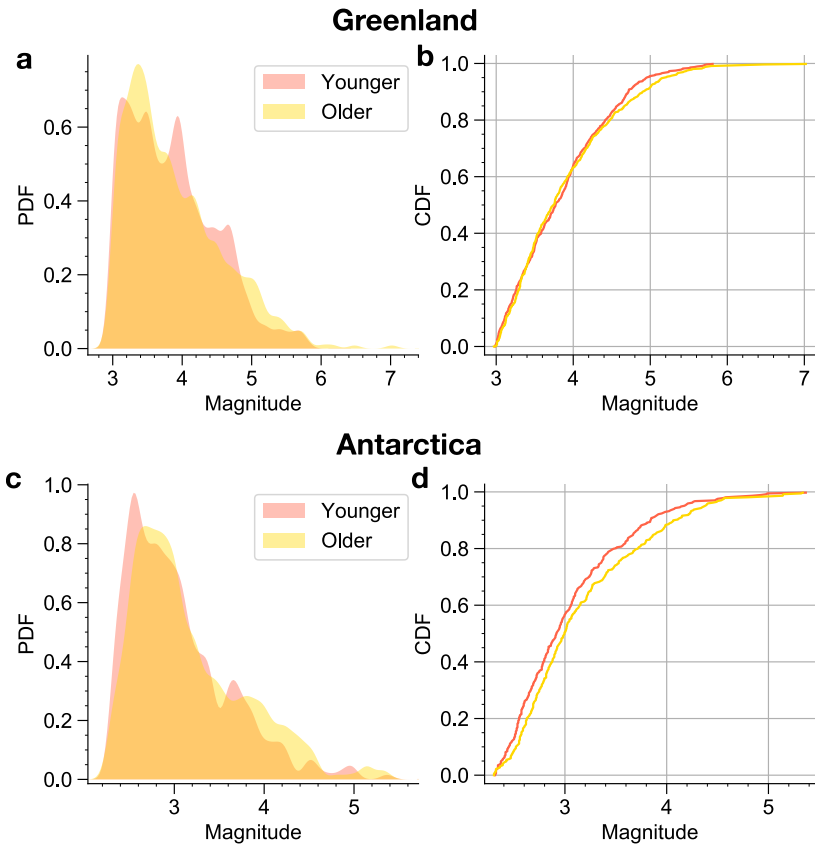

FIG. S8. Distributions of sulfate deposition magnitudes (natural logarithm of the estimated sulfate deposition in kg/km^2) in the unipolar Greenlandic (**a-b**) and Antarctic (**c-d**) data set from Lin et al. (2022), which is split up into the younger and older halves of the eruptions.

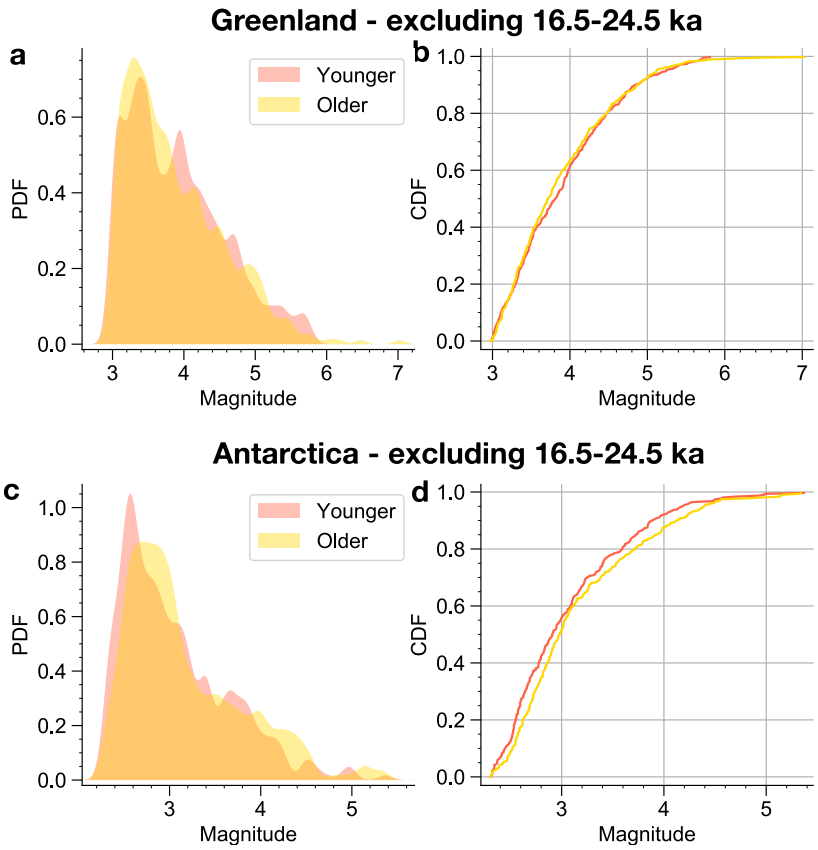

FIG. S9. Same as Fig. S8, but the eruptions in the period 16.5-24.5 ka are excluded. This corresponds to the gap in the bipolar record of Svensson et al. (2020) and it is a period of increased impurity levels in the ice core, which consequently may result in different statistical properties of the eruption record.

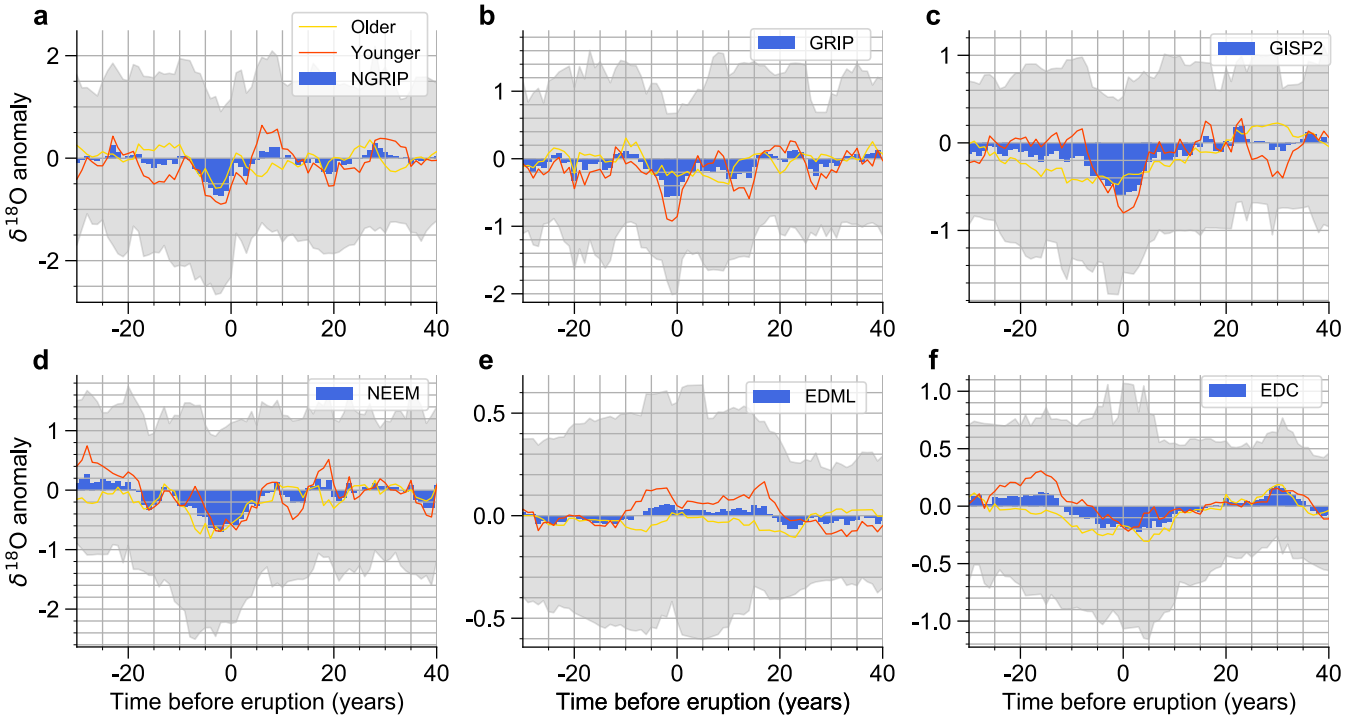

FIG. S10. Average δ^{18}O anomalies (permil) in the individual ice cores aligned to the bipolar eruptions. The gray shading and blue curve are the same as in Fig's. 1, 2, and S5, and the red (yellow) curves correspond to the average δ^{18}O anomaly of the younger (older) half of the bipolar data set. The corresponding curves for the Greenland stack and the WAIS core are shown in Fig. 3.

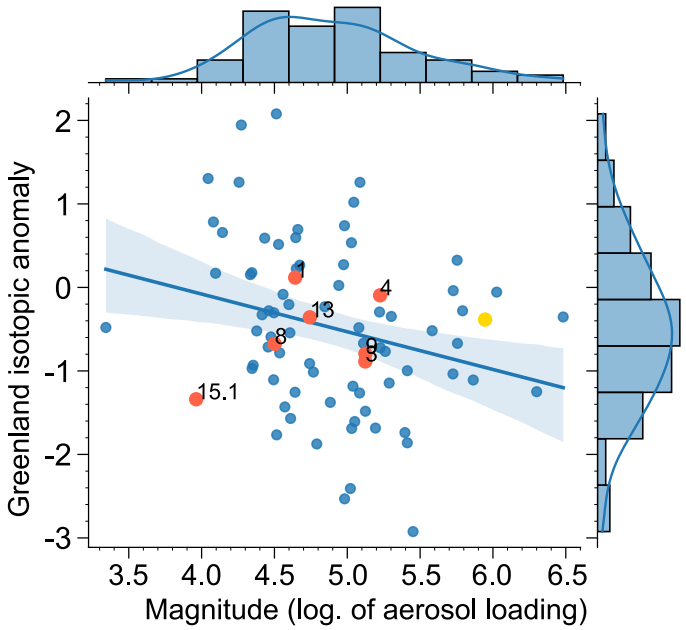

FIG. S11. Correlation of the 6-year anomaly (permil) after bipolar eruptions in the Greenland δ^{18}O stack and the logarithm of the total sulfur aerosol loading (in Tg) derived from the sulfur deposition in the Greenland and Antarctic ice cores (Lin et al. 2022). In red are the eruptions preceding the onsets of Dansgaard-Oeschger events within less than 50 years, as identified in Lohmann and Svensson (2022).

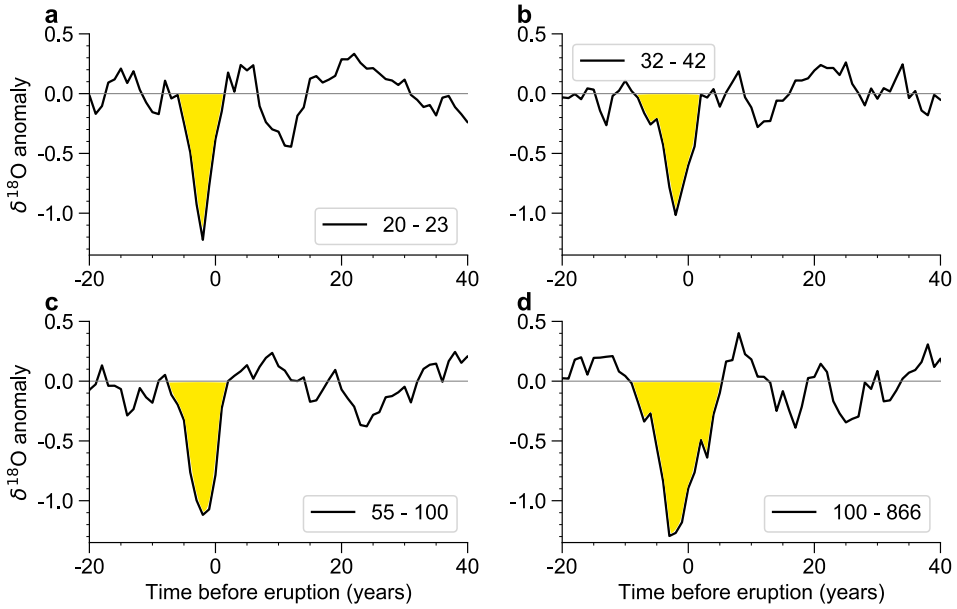

FIG. S12. Mean δ^{18}O anomaly (permil) in NGRIP for the unipolar data set, which is divided into subsets of eruptions with different sulfate deposition magnitude, bounded by the 15-, 30-, 45-, 60-, 75-, and 90-percentiles of the sulfur deposition values. Panels **a-d** show examples of the mean anomaly in four different deposition magnitude bins, corresponding to the 0- to 15-percentile, 30- to 45- percentile, 75- to 90-percentile, and 90- to 100-percentile, respectively. The corresponding range of sulfur deposition values is indicated by the number in the legend (units are kg/km^2). From these average curves, an integrated anomaly is defined by calculating the area shaded in yellow. This integrated anomaly as a function of the median deposition in the respective bin is shown in Fig. 4a for NGRIP, and in Fig. S13 for other ice cores.

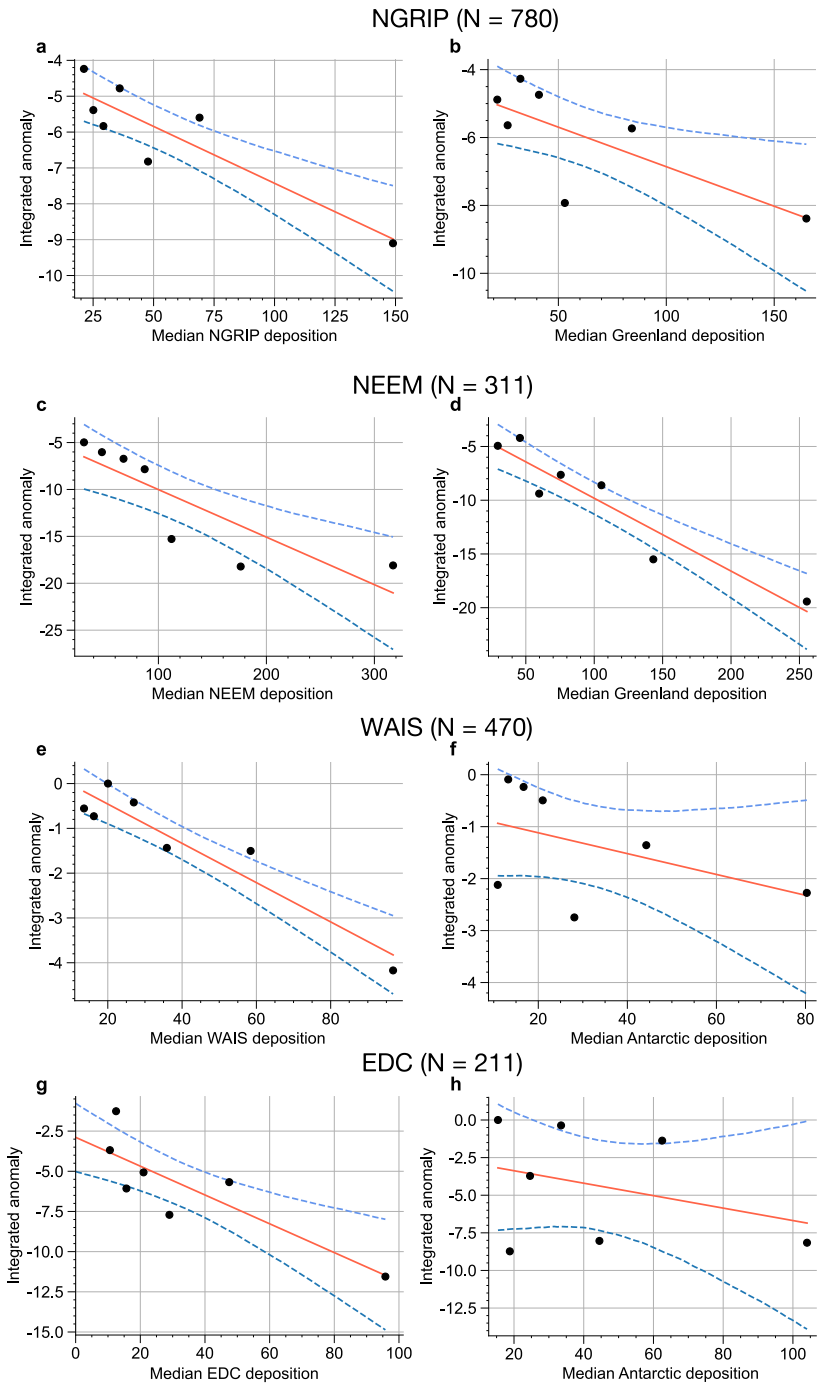

FIG. S13. Correlation of the integrated δ^{18}O anomalies (permil x years) in different ice cores (eruptions from the unipolar dataset) and the associated sulfur deposition. The individual dots are average integrated anomaly in bins according to the sulfur deposition in the individual cores (left column), or to the deposition averaged over all cores of the respective Hemisphere (right column). The integrated anomaly is defined by the sum of averaged δ^{18}O anomaly values in those years around the estimated year of eruption where the anomaly is negative, as shown in Fig. S12. For visual orientation, we also show a linear regression with 95% confidence intervals.

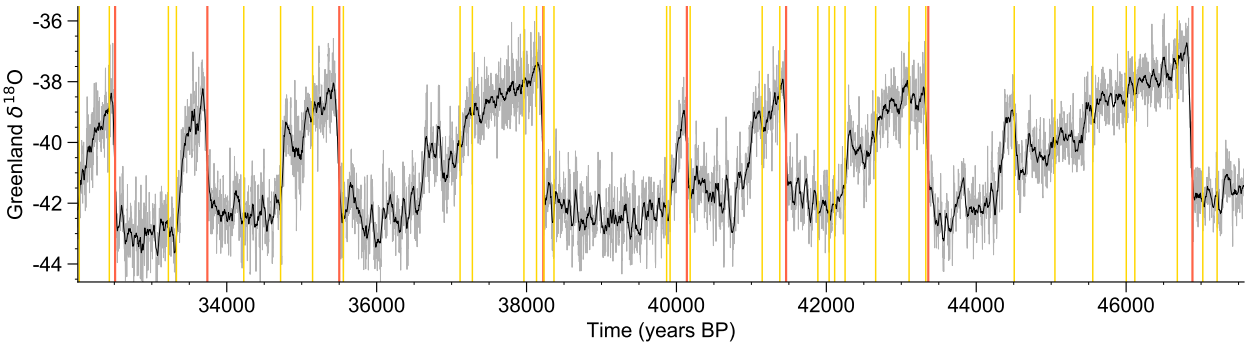

FIG. S14. Time series of the Greenland stacked δ^{18}O record for the time period with an equal duration of stadial and interstadial conditions, as used in Fig. 8e,f. In yellow are the bipolar eruptions from Svensson et al (2020), and in red are estimates of the onsets of Dansgaard-Oeschger warmings from Lohmann and Svensson (2022).

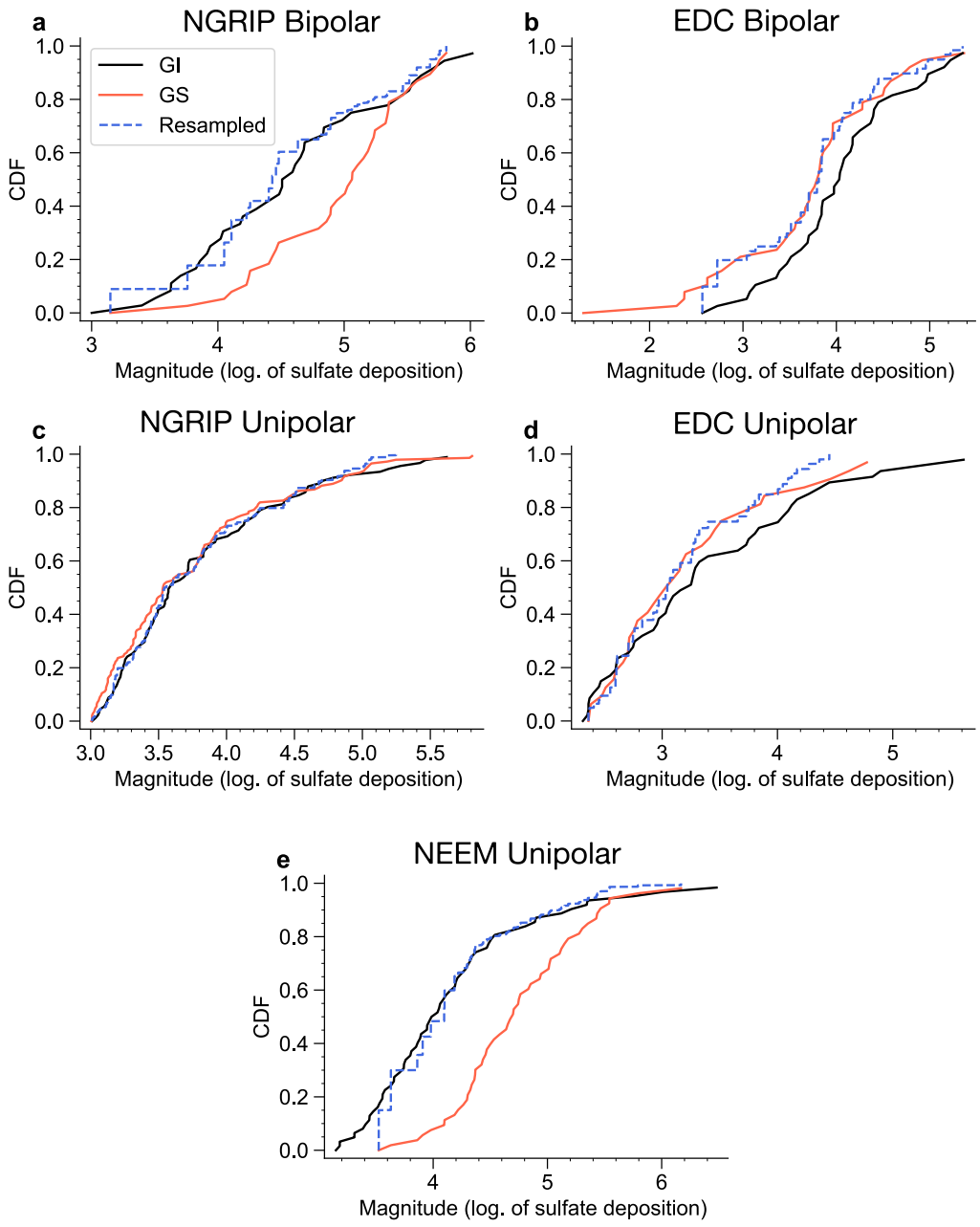

FIG. S15. Cumulative distribution functions of the magnitude of eruptions, separated in eruptions occurring during GI (black) and GS (red). The magnitudes are given as the logarithm of the average sulfate deposition (in kg/km^2) of an eruption in all cores of one pole where the eruption could be detected by Lin et al. (2022). The blue dashed lines show the distribution functions of resampled subsets of eruptions obtained from the GS (GI) population in the Greenland (Antarctic) cores such that they follow the distribution (with lower average magnitudes) of the GI (GS) subset (see main text for more details).

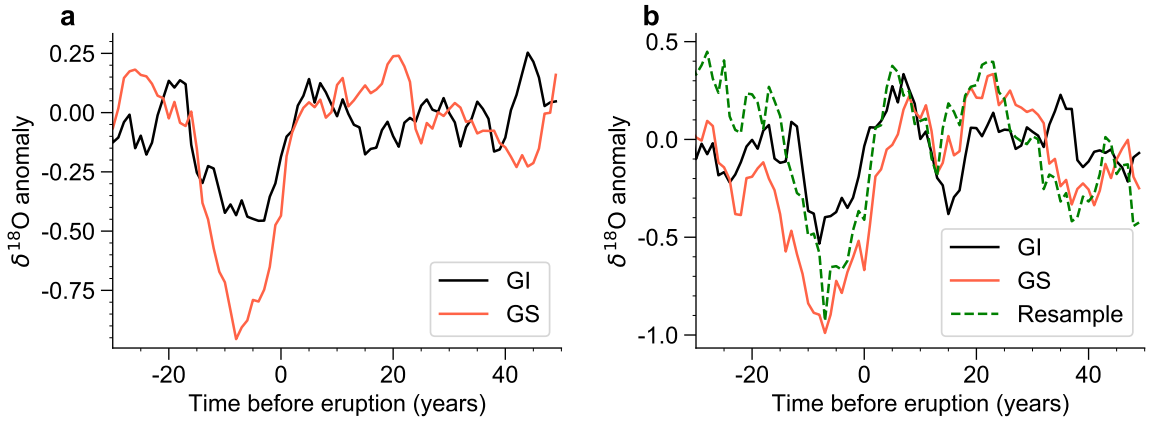

FIG. S16. Same as Fig. 8c,e in the main text, but for the NEEM core.

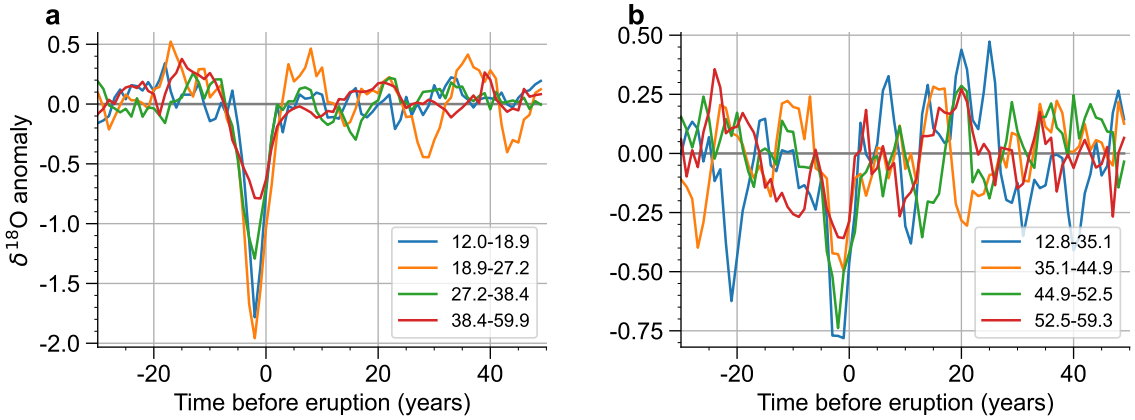

FIG. S17. Mean δ^{18}O anomaly (permil) in NGRIP for eruptions of the unipolar data set occurring during GS (**a**) and GI (**b**). Shown are the average anomalies for equally sized subsets of eruptions divided according to age, which is listed in the legend in kyr.